Published in final edited form as:
Magn Reson Imaging. 2012 February ; 30(2): 261–270. doi:10.1016/j.mri.2011.09.006.

Responses of dopaminergic, serotonergic and noradrenergic networks to acute levo-tetrahydropalmatine administration in naïve rats detected at 9.4 T

Xiping Liu[a], **Zheng Yang**[b], **Rupeng Li**[a], **Jun Xie**[a], **Qian Yin**[a], **Alan S. Bloom**[c], and **Shi-Jiang Li**[a,d,*]

[a]Department of Biophysics, Medical College of Wisconsin, Milwaukee, WI 53226, USA

[b]Beijing Institute of Basic Medical Science, Beijing 100005, China

[c]Department of Pharmacology and Toxicology, Medical College of Wisconsin, Milwaukee, WI 53226, USA

[d]Department of Psychiatry and Behavioral Medicine, Medical College of Wisconsin, Milwaukee, WI 53226, USA

Abstract

Aim—The aim of this study was to understand the neuropharmacological characteristics of levo-tetrahydropalmatine (*l*-THP), a recently found potential treatment for drug addiction, and discover its neural correlates and sites of action.

Methods—High-field pharmacological magnetic resonance imaging (phMRI) was used to detect activation induced by acute *l*-THP administration in the naïve rat brain at dose levels of 5, 10, 20 and 40 mg/kg.

Results—Interestingly, the pharmacological profile of *l*-THP selectively binds to the receptors of the dopaminergic, serotonergic and noradrenergic systems. Using the phMRI method, it was demonstrated that *l*-THP selectively activated the key brain regions of the dopaminergic, serotonergic and noradrenergic systems in a dose-dependent manner.

Conclusion—Numerous studies suggest a critical role of monoamines in the behavioral, pharmacological and addictive properties of psychostimulants. It is suggested that *l*-THP holds great potential to be a therapeutic medication for drug addiction.

Keywords

Levo-tetrahydropalmatine; MRI; BOLD; Pharmacological connectivity

1. Introduction

Recent preclinical and laboratory behavioral studies have demonstrated the great potential of levo-tetrahydropalmatine (*l*-THP) to treat drug addiction, ameliorate withdrawal symptoms and prevent or inhibit relapse. *L*-THP is a purified compound from the Chinese herb corydalis; the latter has been used to treat pain since the fifth century. *L*-THP has been clinically and safely prescribed for about 30 years as an analgesic and hypnotic medication in many fields without showing any abuse potential [1]. Recent preclinical studies showed

*Corresponding author. Tel.: +1 414 456 4029; fax: +1 414 456 6512. sjli@mcw.edu (S.-J. Li).

that *l*-THP inhibits cocaine-induced conditioned place preference behavior and inhibits methamphetamine- and oxycodone-induced discriminative behavior in a dose-dependent manner [2-4]. Most importantly, the agent does not significantly attenuate food response during reinstatement, whereas it significantly attenuates cocaine self-administration and cocaine-induced reinstatement in rats [5]. In addition, *l*-THP inhibits cocaine-enhanced rat brain stimulation rewarding effects [6]. A preliminary clinical study in China indicated that *l*-THP reduced drug craving and increased extinction rates in heroin-dependent subjects [7].

Early mechanistic studies indicated that in addition to being a dopamine (DA) (D_1, and D_2)-receptor antagonist that preferentially blocks the DA D_2 receptors in the striatum and nucleus accumbens (NAc) [8], *l*-THP also interacts with serotonergic and noradrenergic networks [9,10]. The possibility that *l*-THP interacts with all the three monoamine circuits (dopaminergic, serotonergic and noradrenergic) has drawn our interest, as extensive literature documents the critical importance of monoamines in the behavioral, pharmacological and addictive properties of psychostimulants [11-13]. Recent studies demonstrated that the serotonin transmitter system has modulatory function for the limbic-corticostriatal circuitry that is vital in the aspects that hinder recovery and contribute to relapse [14]. Similarly, recent evidence also implicates norepinephrine in stress- and drug-induced reinstatement of extinguished psychostimulant self-administration [15]. It is speculated that if *l*-THP can antagonize these monoamine systems, then the *l*-THP treatment may provide neurochemical normalization therapy for psychostimulant addiction, or other related psychiatric disorders, such as depression, attention deficit and obsessive compulsive disorders. Before we can test this theory, we must clarify the overall pharmacological profile of *l*-THP. We need to find out its neural correlates or sites of action in the brain.

In the present study, we report the results of the pharmacological profile analysis of *l*-THP. Profile data analyses can identify off-target interactions that can help predict the potential side effects, efficacy and safety of *l*-THP. In turn, this reduces the cost incurred before advancing to preclinical and clinical trials. The main purpose of this study was to identify all targeting neuronal substrates of *l*-THP on the naïve rat brain, using pharmacological magnetic resonance imaging (phMRI). These results will serve as baseline information for future studies using diseased models. In addition, they will help us to determine the neurobiological mechanisms of *l*-THP treatment efficacy.

2. Materials and methods

2.1. Pharmacological profile

Competitive binding assay tests across 73 receptors were contracted to NovaScreen Bioscience (Hopkinton, MA, USA), which ran the broad panel of neurotransmitter, growth factor, immunological factor and brain gut peptide receptor binding assays for *l*-THP. Briefly, at a concentration of 10 μM, *l*-THP was tested to compete with the corresponding radioligand for each receptor-binding assay. Two replicates were done and averaged for each receptor. The significant binding activity was defined as inhibition of radioligand binding of 50% or greater.

2.2. Animal and preparation

A total of 22 naïve male Sprague-Dawley rats weighing 300 to 350 g were used in this study. Before the experiment, all rats were given free access to food and water and kept in a home cage with 12 h of day/night light alternation for at least 1 week after shipment. The 22 rats were randomly divided into six groups for three types of scans: four rats were in the control group (Group 1) for scan type 1 (Scan I) and another 12 rats (four in each group) were combined to create four *l*-THP dosage groups: 5, 10, 20 and 40 mg/kg for scan type 2 (Scan II). These doses were selected according to their behavioral effects on cocaine use in

rats [4-6]. To examine if *l*-THP interacts with the μ-opioid receptor, the remaining six rats were involved in a naloxone (μ-opioid receptor competitive antagonist) study in scan type 3 (Scan III). The interval between Scan I and Scan II was about 30 min. All animal experiment protocols and procedures were conducted in accordance with the National Institutes of Health Guide for the Care and Use of Laboratory Animals and approved by the Institutional Animal Care and Use Committee.

Anesthesia was induced with 20% urethane (1.2 g/kg). The right femoral vein and femoral artery were cannulated with PE-50 polyethylene tubing (Becton-Dickinson, Sparks, MD, USA), flushed with heparinized saline before use for intravenous drug delivery and arterial blood pressure monitoring, respectively. Respiratory ventilation was provided by air through an intratracheal Y-shaped Teflon tube at 50 pushes per minute and 2.40 to 2.80 ml of tidal volume via an MRI-1 volume cycled MR-compatible ventilator (CWE, Ardmore, PA, USA). The rats' core temperature was monitored with a rectal thermometer and maintained at 37°C ±1°C by circulating warm water through a custom-built G-10 fiberglass animal holder controlled by a water pump-driven temperature regulator (Medi-therm III; Gaymar Industries, Orchard Park, NY, USA). A small animal monitoring system (Model 1025; SA Instruments, Stony Brook, NY, USA) was used to monitor arterial blood pressure, core temperature and respiratory rate. A pulse oximeter (8600V; Nonin Medical, Plymouth, MN, USA) and inspired/expired O_2 and CO_2 sampler (POET IQ2; Criticare Systems, Waukesha, WI, USA) also were used. Results were recorded with the WinDaq Pro terminal (DataQ Instrument, Akron, OH, USA) and kept within normal physiologic ranges. Gallamine (250 mg/kg), a competitive cholinergic receptor blocker, was slowly administered intravenously 15 min before data acquisition as a muscle relaxant to eliminate spontaneous respirations and minimize motion artifacts.

2.3. MRI image acquisition

A 9.4 T MRI system with a 31-cm horizontal bore (Biospec Avance 94/31; Bruker, Karlsruhe, Germany) was used for scanning. A cylindrical volume coil for radio frequency transmission and an Insight Neuroimaging Systems, LLC, surface coil (Worcester, MA, USA) for MR signal receive were used to image the rat brain. After a quick localization scan with flash sequence, a high-resolution scan was acquired with spin-echo rapid acquisition with relaxation enhancement (RARE) pulse sequence used to acquire images in a sagittal plane to accurately localize the anterior commissure in order to ensure repeatability in slice positioning between different rat brains. After obtaining accurate slice positioning, the same RARE sequence and scanning parameters were used to acquire six slices with the following acquisition parameters: repetition time (TR) of 5000 ms, echo time (TE) of 11.3 ms, number of average of 2, field of view (FOV) of 35×35 mm^2, matrix size of 128×128 and slice thickness of 2 mm in coronal plane. After the high-resolution anatomical scan, phMRI scans were taken with the same setup and scanning parameters, except a TR of 3000 ms (volume repetition time is 24 s), TE of 12.5 ms, single average and matrix size of 64×64 were used. Unlike the echo planer imaging (EPI) sequence, RARE sequence has significantly less susceptibility artifacts in the regions between the air–tissue boundaries. Further, the present pharmacological studies require temporal resolution in minutes instead of a subsecond acquisition in an EPI experiment. Therefore, a RARE sequence was used for this study.

As shown in Fig. 1, all three scan types lasted 60 min (150 repetitions). In Scan I, distilled water (0.3 ml in 40 s) and saline vehicles (0.3 ml in 40 s) were intravenously infused 5 and 25 min into the 60-min scan, respectively. Distilled water was used, because *l*-THP was dissolved in it, but not in the physiological solution. All drugs were dissolved in 0.3 ml and intravenously infused in 40 s. In Scan II, *l*-THP (four different doses) was infused at 5 min into the 60-min scan. In Scan III, *l*-THP (40 mg/kg) and naloxone (4 mg/kg) were infused 5

and 25 min into the 60-min scan. All rats were finally euthanized with an overdose of pentobarbital after experiments.

2.4. Data analysis

An Analysis of Functional NeuroImages (AFNI) software package (National Institutes of Health [NIH], Baltimore, MD, USA) was used for image analysis. Four-dimensional PhMRI data sets of individual rats were first coregistered onto the corresponding high-resolution anatomical RARE images. Then, a time series of each voxel was temporally smoothed with a 5-point Hamming window. According to the pharmacological and functional response character, the blood oxygen level-dependent (BOLD) phMRI signals of Scans I and II in each voxel of every individual animal were fitted with a nonlinear Beta model, as shown in Eq. (1) [16]:

$$y(t)=k\left(\frac{t-t_0}{t_f-t_0}\right)^{\alpha-1}\left(\frac{t_f-t}{t_f-t_0}\right)^{\beta-1} \quad to<t<t_f \tag{1}$$

where t_0 is the time delay of response after drug injection, t_f is the end time of response, k is a multiplicative coefficient, and α and β are parameters of the β distribution. The initial values to be fitted for parameters t_0, t_f, k, α and β were set to 0–5 min, 5–60 min, 1000–10,000, 0–10 and 0–10, respectively. All initial values of those parameters were chosen loosely enough to accommodate the best fit of time-course data in various locations. Because the k value can be positive or negative, the voxelwise signal can be either positive or negative. A two-tailed Student's t test was used for statistical analyses of phMRI data. The voxelwise area under the curve (AUC%) in each *l*-THP dose group from Scan II was compared to that of the control group from Scan I. The statistical significance for activated voxels in phMRI data was operationally defined as clusterwise $P<.05$, with a minimum cluster size of 19 voxels and a voxel size of $0.55\times0.55\times2$ mm^3. One-way analysis of the variance (ANOVA) method was used to differentiate the dose responses of the voxelwise AUC% values of BOLD signals in various *l*-THP dosage groups. Significantly dose-dependent voxels had a threshold of $F>5.67$ (clusterwise, $P<.01$) with a minimum cluster size of eight voxels. For Scan III, signal intensity in a time course of 5 min before and after naloxone injection was averaged, and the difference between the two mean values was compared with that from the control group (Scan I). The changes were also tested by using a groupwise t test that evaluated the voxelwise AUC% values after naloxone infusion (25–60 min) in Scan III as compared to those in the non-naloxone Scan II.

The anatomical image set of one rat was chosen as a reference template. FMRIB's Linear Image Registration Tool (FLIRT) program in FMRIB Software Library (FSL) software [17] was used to register all of the rats' AUC% images onto the reference template. Medical Image Visualization and Analysis (MIVA) software (Center for Comparative NeuroImaging, Worcester, MA, USA) was used to segment the reference template images completely into 43 regions of interest (ROIs) (demonstrated in Fig. 3). All phMRI activation maps, as well as the *l*-THP dose-dependent map, were overlaid on the corresponding anatomical images to show the localization of neuronal activity. The ROI-segmented dose-dependent map and least-square linear regression were further applied to evaluate the dose response of regional AUC% values. To demonstrate the regional linear correlation of the *l*-THP dose and AUC% value, the Pearson correlation coefficient was acquired with a statistical significance threshold of clusterwise $P<.05$ and a minimum cluster size of 19 voxels.

To further generate pharmacological connectivity maps, four ROIs—ventral tegmental area (VTA), raphe nuclei, bed nucleus of stria terminalis (BNST) and a control region,

pedunculopontine tegmental nucleus (PPT)—were chosen as the seed regions. For each seed ROI, an averaged BOLD signal (AUC%) can be obtained from each rat. As a result, the 16 BOLD signals in a specific ROI from the 16 rats can form a seed vector (1×16). The seed vector was cross-correlated with the voxelwise AUC% values across the 16 rats throughout the whole brain, as shown in Eq. (2) [18].

$$r=\frac{\sum_{i=1}^{n}(x_i-\bar{x})(y_i-\bar{y})}{\sqrt{\sum_{i-1}^{n}(x_i-\bar{x})^2\sum_{i-1}^{n}(y_i-\bar{y})^2}} \quad (2)$$

where $\{x_i: i=1\ldots n\}$ and $\{y_i: i=1\ldots n\}$ are the time series from two voxels, and $\bar{x}$ and $\bar{y}$ correspond to the time averages of $\{x_i\}$ and $\{y_i\}$, respectively. Finally, correlation coefficient maps were transformed into a z map and clustered with a minimum cluster size of 8 voxels (clusterwise $P<.05$).

3. Results

As listed in Table 1, among the 73 tested neurotransmitter-related receptors, *l*-THP has a significant high binding affinity (inhibition of 50% or greater of the radioligand binding) for α1A- and α2A-adrenergic receptors; D1, D2, and D3 receptors and several serotonin (5-hydroxytryptamine; 5-HT) receptors (5-HT1A, 5-HT1D, 5-HT4 and 5-HT7) (shown in bold in Table 1). There is no significant binding activity for the rest of the receptors tested including the cannabinoid, muscarinic and opioid receptors.

There were brief alterations in the mean arterial blood pressure (a 7% decrease for 40 mg/kg) and peripheral oxygen saturation levels (a 3% increase for 40 mg/kg) at 30 s after *l*-THP infusion, which were recovered within the first minute. The heart rate did drop significantly (30% for 40 mg/kg) within the first minute but recovered within 3 min after infusion. As blood pressure was maintained well above the autoregulation threshold, the transient change of physiological parameters should confound minimally on the AUC% measurement for the entire 60-min scan.

Fig. 2 shows the time courses of one animal as related to regional brain responses to the vehicle, *l*-THP and naloxone infusions during the 60-min scanning time. The brain responses to *l*-THP infusion (40 mg/kg) lasted for more than 40 min for most regions. Acute *l*-THP infusion-induced negative BOLD signal in reward- and addiction-related regions, such as NAc, infralimbic cortex (IL; ventromedial prefrontal cortex) and VTA, compared with that in the control group. No significant BOLD change was found in the claustrum (Cl) (also in Table 2). To test the interaction of *l*-THP with μ-opioid receptor, naloxone, a competitive μ-opioid receptor antagonist, was infused at 25 min after *l*-THP during Scan III. Naloxone itself has been found to elicit BOLD increase in the somatosensory region of normal rats [19]. In the current study, there were no significant BOLD signal changes after the naloxone infusion. Likewise, there were no significant AUC% changes for 25–60 min of Scan III compared to that of Scan II ($P<.05$). These results may suggest that *l*-THP does not work directly on μ-receptor. Alternatively, we cannot exclude the possibility that the *l*-THP may block the naloxone-induced BOLD effect.

Fig. 3 shows the dose-response maps (row A for a dose of 5 mg/kg, row B for 10 mg/kg, row C for 20 mg/kg and row D for 40 mg/kg). Different doses of *l*-THP showed varied activation maps. From A to D, within each dose group, the AUC% values of *l*-THP-induced voxelwise BOLD responses were tested (*t* test) with the AUC% values in the vehicle group to generate the corresponding dose-response map. Fig. 3E shows the rat anatomy as a

reference for locating the brain regions in the activation maps. The *l*-THP dose-dependent map was generated with a one-way ANOVA test of voxelwise AUC% values in all (vehicle and *l*-THP) groups, with a threshold of $F>5.67$ (clusterwise $P<.01$) and a minimum cluster size of 8 voxels. Fig. 3F shows the dose-dependent map of *l*-THP treatment. After segmentation, 14 ROIs were found to be *l*-THP dose-dependent, as listed in Table 2. The mean AUC% values in *l*-THP dose-dependent ROIs of various dose groups were also listed. The higher the *l*-THP dose, the higher the BOLD signal responses (more negative). With regional analysis, many highly addiction-related ROIs were revealed to be *l*-THP dose-dependent. These include the NAc, substantia nigra (SNR), insular cortex (Ins), hippocampus (HIPP), IL, retrosplenium, VTA, thalamus (Thal), hypothalamus (Hypoth), caudate/putamen (CPu) and BNST. The regional AUC% values were significantly linearly correlated with *l*-THP doses, as demonstrated in Fig. 4.

Fig. 5 demonstrates the connectivity maps activated by *l*-THP infusion. A for VTA, B for raphe and C for BNST show that distinctly different neuronal circuits were depicted when different seed regions were applied. When the VTA, the primary source of DA, was used as the seed region the highly related regions of DA, such as the olfactory cortex, insula, CPu, amygdala (Amy) and HIPP were revealed. When raphe nucleus, the primary source of 5-HT, was chosen as the seed region, a few regions like the somatosensory cortex, CPu, HIPP and periaqueductal gray matter were revealed. When BNST was used as the seed region, broad regions, including the cingulate cortex, motor cortex, somatosensory cortex, NAc, CPu, insula, Amy, Thal, Hypoth, HIPP and retrosplenium cortex were revealed. When the primary cholinergic source PPT was chosen as the seed, only a small area of the somatosensory cortex was revealed (as in Fig. 5). Row D in Fig. 5 shows the common regions of Fig. 5A–C. Red represents the common areas of the VTA and raphe connectivity maps; yellow represents the areas common to VTA and BNST maps; blue represents the areas common to raphe and BNST maps and green represents the areas common to all three maps.

4. Discussion

The present study demonstrated two major findings: the pharmacological profile of *l*-THP and its dose-dependent regional activation. Pharmacology profiling has become an invaluable tool in identifying off-target interaction and predicting potential treatment efficacy and safety. The pharmacological profiling of *l*-THP, as listed in Table 1, indicates its high-affinity binding to α1- and α2-adrenergic receptors; D1, D2, and D3 receptors and several serotonin (5-hydroxytryptamine; 5-HT) receptors (5-HT1A, 5-HT1D, 5-HT4 and 5-HT7). Accordingly, Zhang and colleagues [20] found that *l*-THP behaves as a D1, D2 antagonist for isolated rabbit peripheral artery. Liu et al. [9] found *l*-THP to be monoamine depletor. Future in vitro study of *l*-THP on these monoamine systems will confirm its actual functional effects.

With high-field phMRI, acute *l*-THP elicited a dose-dependent negative BOLD response in specific regions that are highly addiction related. These include the NAc, SNR, Ins, HIPP, IL, retrosplenium, VTA, Thal, Hypoth and CPu. Current pharmacotherapy concepts related to drug dependence have focused on preventing relapse, rather than disrupting primary reinforcement. Many studies have shown that all these regions play critical roles for drug addiction and behave as key neural substrates involved in drug relapse [11]. The NAc [21] appears to be involved in the primary reinforcing effects of drug abuse. The VTA is believed to be extensively involved in mediating the rewarding effects, conscious drug experience and drug-seeking behavior [22]. The Ins has recently been implied in playing an important role in cue-induced drug craving [23]. The HIPP takes major responsibility in conditioned learning engaged in the process of addiction [24]. IL appears to be involved in drug-primed

reinstatement in a drug-dependent fashion [25]. The SNR is particularly important in motor planning, reward-seeking, learning and withdrawal [26]. The CPu does not seem to have a major role in the acute reinforcing effects of drug abuse, but may be recruited during the development of compulsive drug seeking [27]. The retrosplenium (posterior cingulate cortex in human) is also involved and implicated in inhibitory control and conflict resolution. Its disruption results in impulsivity [28]. As drugs with multiple receptor targets have been suggested for the treatment of addiction, *l*-THP proves to be unique in that it exclusively binds to major receptors of the dopaminergic, serotonergic and noradrenergic networks. This highlights its great potential as a therapeutic medication for addiction.

Although we did not find significant direct-binding affinity of *l*-THP with opioid receptors (as in Table 1), and naloxone (μ-opioid receptor competitive antagonist) did not change the *l*-THP -induced BOLD responses, previous studies have demonstrated that the *l*-THP can modulate the opioid system indirectly. Jin [1] and Hu and Jin [29] found that *l*-THP injection significantly increased the amount of endogenous opioids (mainly endorphins, enkephalins and dynorphins), as well as the messenger RNA expression of the opioid precursor in widespread regions of the central nervous system. Therefore, *l*-THP may enhance opioid activity through interaction with the above-mentioned monoamine neural substrates.

The functional connectivity analysis results on the dopaminergic, serotonergic and noradrenergic networks support the drug profile of *l*-THP binding to those monoamine receptors selectively and provide supplementary network information for the regional patterns of dose-dependent activation of *l*-THP. There have been similar methods in many positron emission tomography and recent phMRI studies [30]. We calculated the acute *l*-THP administration-induced pharmacological connectivity maps, as shown in Fig. 5. The results demonstrated that distinctly different neural circuits were depicted when different seed regions were applied. Using the seed region of VTA, the primary source of DA revealed some DA neurons in highly innervated regions, such as the olfactory cortex, insula, CPu, Amy and HIPP. Interestingly, the NAc region was not found in this connective map, although NAc receives innervations from the VTA. The lack of significant correlation between the VTA and NAc may be due to the variability in responses by individual rats and a relatively a small number of subjects. It is also possible that the activity in the NAc may be influenced not only by the VTA, but also by other circuitry. The seed region of raphe nucleus, the primary source of 5-HT, linked the somatosensory cortex, CPu, HIPP, periaqueductal gray matter, etc. Although there are 5-HT projections spread throughout the brain, many of those regions were dominant distribution areas of other circuits. Because our image acquisition did not cover the locus ceruleus, the primary source of norepinephrine, the seed region of BNST instead was used. The BNST is where drug abuse promotes robust rises in extracellular DA levels. It is a corticotrophin-releasing factor-rich component of the extended Amy. The BNST was connected to a series of regions, including the cingulate cortex, motor cortex, somatosensory cortex, NAc, CPu, insula, Amy, Thal, Hypoth, HIPP and retrosplenium cortex. When the primary cholinergic source PPT was chosen as the control seed, only a small area of the somatosensory cortex was revealed. It supports the low-binding activity of *l*-THP with all muscarinic receptors. Overall, these results support the pharmacological profile of *l*-THP binding with the dopaminergic, serotonergic and noradrenergic receptors and may suggest the network details of its neural substrates revealed with the dose-dependent BOLD changes. However, extra caution should be taken. Although regions, such as the VTA, BNST and raphe nucleus, can be defined as the origins or hubs of their respective neurotransmitter systems, other neural systems, such as glutamergic system, also exist in these regions. Therefore, observed connectivity patterns may reflect the overall activities in these neural systems induced by *l*-THP.

In this study, we observed consistent negative BOLD signal changes across all *l*-THP dose groups. The underlying mechanisms for the negative BOLD signal observed in this study are not known. In the literature, simultaneous fMRI acquisition and electrophysiological recordings methods suggest that the negative BOLD responses were associated with regional neuronal activity decreases measured by the decreased local field potentials and multiunit activity [31]. These results are in line with several other findings of negative BOLD signal changes obtained in fMRI experiments, which have reflected functionally effective inhibition or suppression of neuronal firing patterns [32]. The negative BOLD signal responses found in the human anterior cingulate cortex are reported to be correlated with local GABA concentrations [33]. Region-specific negative BOLD responses are frequently found in human and animal phMRI studies that use agents such as cocaine, heroin and methylphenidate [34,35]. The heroin-induced negative BOLD changes in the NAc were shown to be correlated with heroin-induced inhibitory neural activity measured by the electroencephalograph (EEG) method. The heroin-induced decrease in cerebral blood flow was measured by laser Doppler flowmetry [36]. It was also suggested that the negative BOLD responses induced by cocaine on human subjects observed in the mesolimbic circuitry may be attributed to DA-induced inhibition [37]. Other studies [38] have suggested that synaptic excitation may work as the main driving force for the blood flow or positive BOLD signal, whereas synaptic inhibition may suppress the increase in intracellular calcium that may abolish the activation-induced increases in blood flow and subsequently decrease the BOLD signal. The relationships between the neural activity and the BOLD signal changes can be rather complicated while examining the effects of monosynaptic excitation, disynaptic inhibition and deactivation on neural activity and CBF [39]. In the present study, we attribute the negative BOLD signals induced by *l*-THP administration to the inhibitory functions, because *l*-THP induced a decrease in neuronal activity in many subcortical regions, as well as in the spinal cord, according to EEG measurements [1]. Therefore, the *l*-THP -induced negative BOLD responses may contribute to its therapeutic efficacy for addiction in the manner that they decrease the reward output via inhibition at the NAc and VTA. They also disrupt the conditional learning formed by the HIPP. This conditional learning is critical for primary rewarding and relapse. The responses further decrease the reward-seeking behavior via SNR and CPu and disconnect the information relay through the Thal during addiction. In addition, the sedative, but non-abusive properties [1] of *l*-THP, may decrease the anxiety and impulsivity that is associated with addiction.

Of note, the negative BOLD signal may be related to the anesthetic agent urethane as it inhibits multiple cellular-signaling channels [40]. Although the vehicle study provided control, there is a possibility that the observed negative BOLD profiles may be associated with the combined effects of *l*-THP and the anesthetic. As previously demonstrated, the BOLD signal can be affected by the different levels of anesthesia or by different anesthetic agents in functional MRI studies [41,42]. In the future, we will address how the *l*-THP-induced BOLD signal and connectivity patterns may be altered by different anesthesia.

In conclusion, preclinical and clinical studies have demonstrated great potential for *l*-THP to treat drug addiction. The present study indicated that the overall pharmacological profile of *l*-THP showed strong binding to the receptors of the dopaminergic, serotonergic and noradrenergic systems. Furthermore, phMRI experiments detected activation induced by acute *l*-THP administration in a dose-dependent region-specific manner. It is suggested that *l*-THP holds great promise to be a therapeutic medication for drug addiction.

Acknowledgments

We thank Ms. Carrie M. O'Connor, M.A., for editorial assistance, Mr. B. Douglas Ward, M.S., for discussions related to statistical analysis. This work was supported by the following National Institutes of Health grant: R01 EB001820 (SJL).

References

1. Jin, GZ. Discoveries in the voyage of corydalis research. Shanghai: Shanghai Science & Techonology; 2001.
2. Luo JY, et al. The effect of l-tetrahydropalmatine on cocaine induced conditioned place preference. Chin J Drug Depend. 2003; (12):177–9.
3. Ren Y, et al. Levo-tetrahydropalmatine inhibits the expression of methamphetamine-induced conditioned place preference in rats. Chin J Drug Depend. 2000; (9):182–6.
4. Liu YL, et al. Levo-tetrahydropalmatine attenuates oxycodone-induced conditioned place preference in rats. Eur J Pharmacol. 2009; 602(2-3):321–7. [PubMed: 19071107]
5. Mantsch JR, et al. Levo-tetrahydropalmatine attenuates cocaine self-administration and cocaine-induced reinstatement in rats. Psychopharmacology (Berl). 2007; 192(4):581–91. [PubMed: 17361394]
6. Xi ZX, et al. Levo-tetrahydropalmatine inhibits cocaine's rewarding effects: experiments with self-administration and brain-stimulation reward in rats. Neuropharmacology. 2007; 53(6):771–82. [PubMed: 17888459]
7. Yang Z, et al. Medication of l-tetrahydropalmatine significantly ameliorates opiate craving and increases the abstinence rate in heroin users: a pilot study. Acta Pharmacol Sin. 2008; 29(7):781–8. [PubMed: 18565275]
8. Marcenac F, Jin GZ, Gonon F. Effect of l-tetrahydropalmatine on dopamine release and metabolism in the rat striatum. Psychopharmacology (Berl). 1986; 89(1):89–93. [PubMed: 3090599]
9. Liu GQ, Algeri S, Garattini S. d-l-tetrahydropalmatine as monoamine depletor. Arch Int Pharmacodyn Ther. 1982; 258(1):39–50. [PubMed: 6182845]
10. Chueh FY, et al. Hypotensive and bradycardic effects of dl-tetrahydropalmatine mediated by decrease in hypothalamic serotonin release in the rat. Jpn J Pharmacol. 1995; 69(2):177–80. [PubMed: 8569056]
11. Howell LL, Kimmel HL. Monoamine transporters and psychostimulant addiction. Biochem Pharmacol. 2008; 75(1):196–217. [PubMed: 17825265]
12. Guillem K, et al. Monoamine oxidase inhibition dramatically increases the motivation to self-administer nicotine in rats. J Neurosci. 2005; 25(38):8593–600. [PubMed: 16177026]
13. Gardner EL, et al. A slow-onset, long-duration indanamine monoamine reuptake inhibitor as a potential maintenance pharmacotherapy for psychostimulant abuse: effects in laboratory rat models relating to addiction. Neuropharmacology. 2006; 51(5):993–1003. [PubMed: 16901516]
14. Bubar MJ, Cunningham KA. Prospects for serotonin 5-HT2R pharmacotherapy in psychostimulant abuse. Prog Brain Res. 2008; 172:319–46. [PubMed: 18772040]
15. Salomon L, et al. Behavioral sensitization to amphetamine results from an uncoupling between noradrenergic and serotonergic neurons. Proc Natl Acad Sci U S A. 2006; 103(19):7476–81. [PubMed: 16648258]
16. Garren ST, Smith RL, Piegorsch WW. On a likelihood-based goodness-of-fit test of the beta-binomial model. Biometrics. 2000; 56(3):947–50. [PubMed: 10985242]
17. Jenkinson M, Smith S. A global optimisation method for robust affine registration of brain images. Med Image Anal. 2001; 5(2):143–56. [PubMed: 11516708]
18. Xu G, et al. Task-modulation of functional synchrony between spontaneous low-frequency oscillations in the human brain detected by fMRI. Magn Reson Med. 2006; 56(1):41–50. [PubMed: 16767759]
19. Endo T, et al. Functional MRI of the brain detects neuropathic pain in experimental spinal cord injury. Pain. 2008; 138(2):292–300. [PubMed: 18258366]

20. Zhang WF, et al. Effects of on tetrahydropalmatine peripheral vascular dopamine DA1 and DA2 receptor subtypes. China Journal of Chinese Materia Medica. 2000; 25(8):498–500.
21. Di Chiara G. From rats to humans and return: testing addiction hypotheses by combined PET imaging and self-reported measures of psychostimulant effects. Commentary on Volkow et al. 'Role of dopamine in drug reinforcement and addiction in humans: results from imaging studies'. Behav Pharmacol. 2002; 13(5-6):371–7. [PubMed: 12394413]
22. Wise RA. Brain reward circuitry: insights from unsensed incentives. Neuron. 2002; 36(2):229–40. [PubMed: 12383779]
23. Contreras M, Ceric F, Torrealba F. Inactivation of the interoceptive insula disrupts drug craving and malaise induced by lithium. Science. 2007; 318(5850):655–8. [PubMed: 17962567]
24. Rogers JL, See RE. Selective inactivation of the ventral hippocampus attenuates cue-induced and cocaine-primed reinstatement of drug-seeking in rats. Neurobiol Learn Mem. 2007; 87(4):688–92. [PubMed: 17337218]
25. Lasseter HC, et al. Prefrontal cortical regulation of drug seeking in animal models of drug relapse. Curr Top Behav Neurosci. 2010; 3:101–17. [PubMed: 21161751]
26. See RE, Elliott JC, Feltenstein MW. The role of dorsal vs ventral striatal pathways in cocaine-seeking behavior after prolonged abstinence in rats. Psychopharmacology (Berl). 2007; 194(3): 321–31. [PubMed: 17589830]
27. Everitt BJ, et al. Review. Neural mechanisms underlying the vulnerability to develop compulsive drug-seeking habits and addiction. Philos Trans R Soc Lond B Biol Sci. 2008; 363(1507):3125–35. [PubMed: 18640910]
28. Volkow ND, Fowler JS, Wang GJ. The addicted human brain viewed in the light of imaging studies: brain circuits and treatment strategies. Neuropharmacology. 2004; 47(Suppl 1):3–13. [PubMed: 15464121]
29. Hu JY, Jin GZ. Supraspinal D2 receptor involved in antinociception induced by l-tetrahydropalmatine. Zhongguo Yao Li Xue Bao. 1999; 20(8):715–9. [PubMed: 10678104]
30. Schwarz AJ, et al. Functional connectivity in the pharmacologically activated brain: resolving networks of correlated responses to d-amphetamine. Magn Reson Med. 2007; 57(4):704–13. [PubMed: 17390353]
31. Shmuel A, et al. Negative functional MRI response correlates with decreases in neuronal activity in monkey visual area V1. Nat Neurosci. 2006; 9(4):569–77. [PubMed: 16547508]
32. Kastrup A, et al. Behavioral correlates of negative BOLD signal changes in the primary somatosensory cortex. Neuroimage. 2008; 41(4):1364–71. [PubMed: 18495495]
33. Northoff G, et al. GABA concentrations in the human anterior cingulate cortex predict negative BOLD responses in fMRI. Nat Neurosci. 2007; 10(12):1515–7. [PubMed: 17982452]
34. Luo F, et al. Attenuation of brain response to heroin correlates with the reinstatement of heroin-seeking in rats by fMRI. Neuroimage. 2004; 22(3):1328–35. [PubMed: 15219605]
35. Febo M, et al. Imaging cocaine-induced changes in the mesocorticolimbic dopaminergic system of conscious rats. J Neurosci Methods. 2004; 139(2):167–76. [PubMed: 15488229]
36. Li SJ, et al. Heroin-induced negative BOLD signal in the nucleus accumbens of rat brain is related to neuronal inhibition. Proc Int Soc Magn Reson Med. 2003; 11:358.
37. Kufahl PR, et al. Neural responses to acute cocaine administration in the human brain detected by fMRI. Neuroimage. 2005; 28(4):904–14. [PubMed: 16061398]
38. Lauritzen M. Reading vascular changes in brain imaging: is dendritic calcium the key? Nat Rev Neurosci. 2005; 6(1):77–85. [PubMed: 15611729]
39. Lauritzen M, Gold L. Brain function and neurophysiological correlates of signals used in functional neuroimaging. J Neurosci. 2003; 23(10):3972–80. [PubMed: 12764081]
40. Hara K, Harris RA. The anesthetic mechanism of urethane: the effects on neurotransmitter-gated ion channels. Anesth Analg. 2002; 94(2):313–8. table of contents. [PubMed: 11812690]
41. Sommers MG, et al. Isoflurane anesthesia is a valuable alternative for alpha-chloralose anesthesia in the forepaw stimulation model in rats. NMR Biomed. 2009; 22(4):414–8. [PubMed: 19003937]

42. Schmidt KF, et al. Hemodynamic and metabolic changes induced by cocaine in anesthetized rat observed with multimodal functional MRI. Psychopharmacology (Berl). 2006; 185(4):479–86. [PubMed: 16550388]

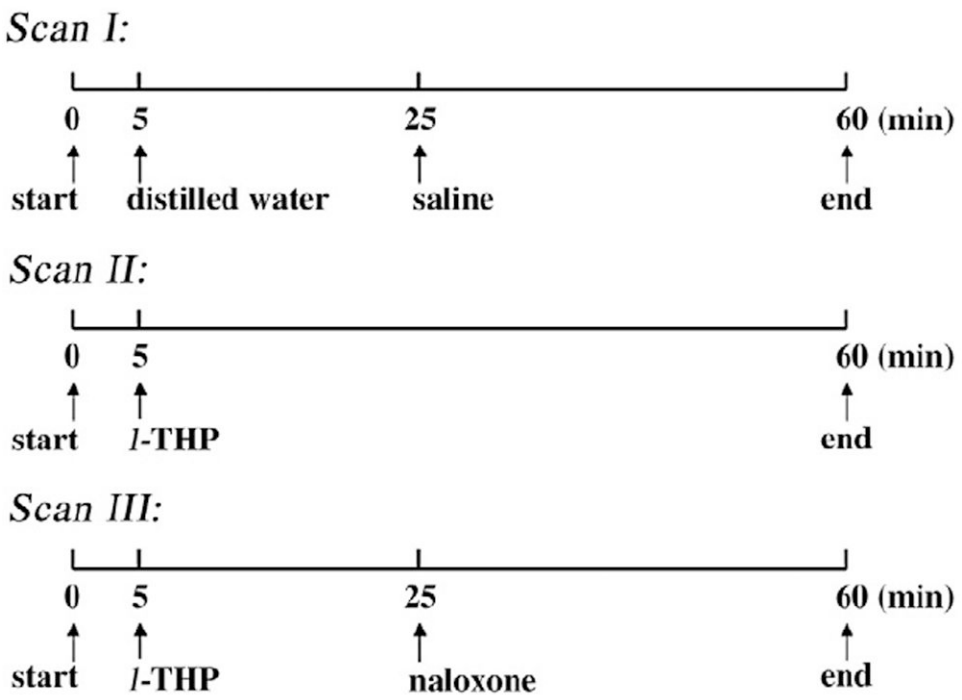

Fig. 1.

Schematic timeline design of three phMRI scans. Distilled water/ *l*-THP was intravenously infused at the 5th minute into the 60-min scan in Scans I to III, and saline/naloxone was intravenously infused at the 25th minute into the 60-min scan of Scans I and III.

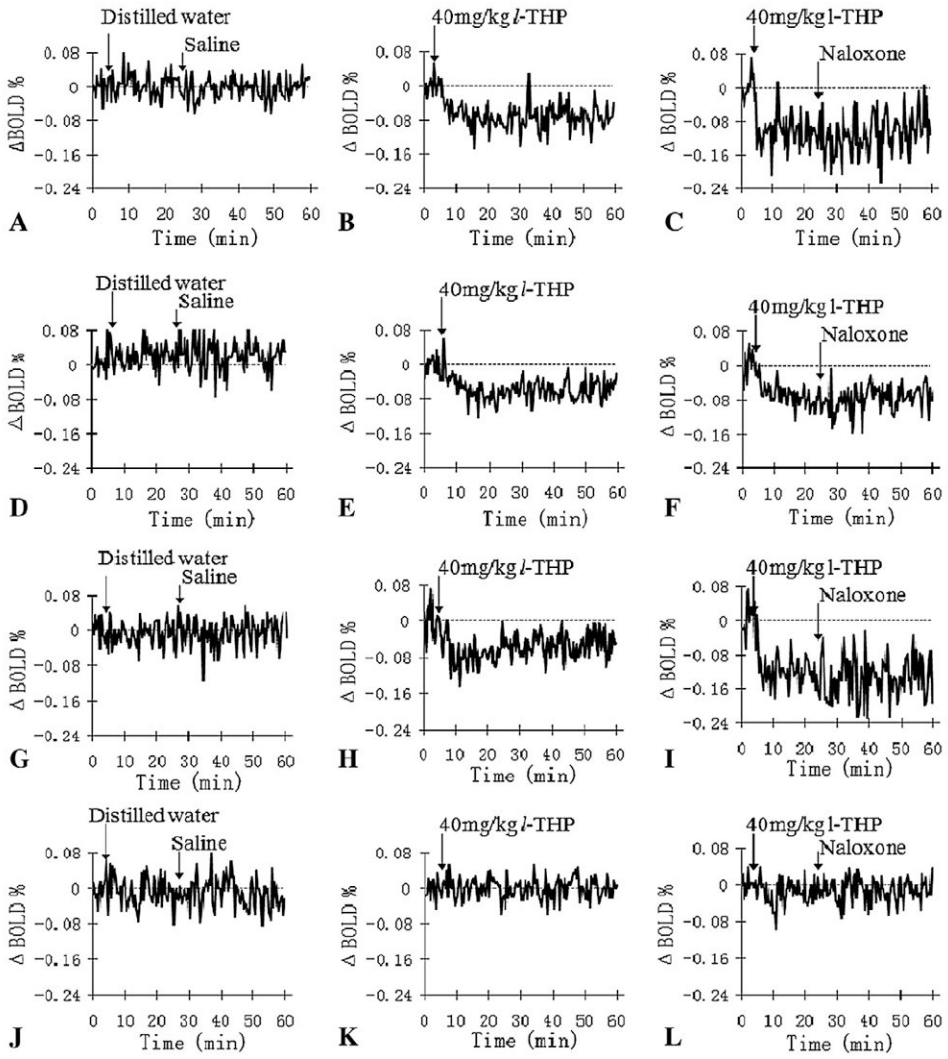

Fig. 2.

Representative relative voxel time course changes (ΔBOLD %) in regions of NAc (A–C), the IL (D–F), VTA (G–I) and Cl (J– L) after the vehicles, *l*-THP and naloxone infusions, respectively.

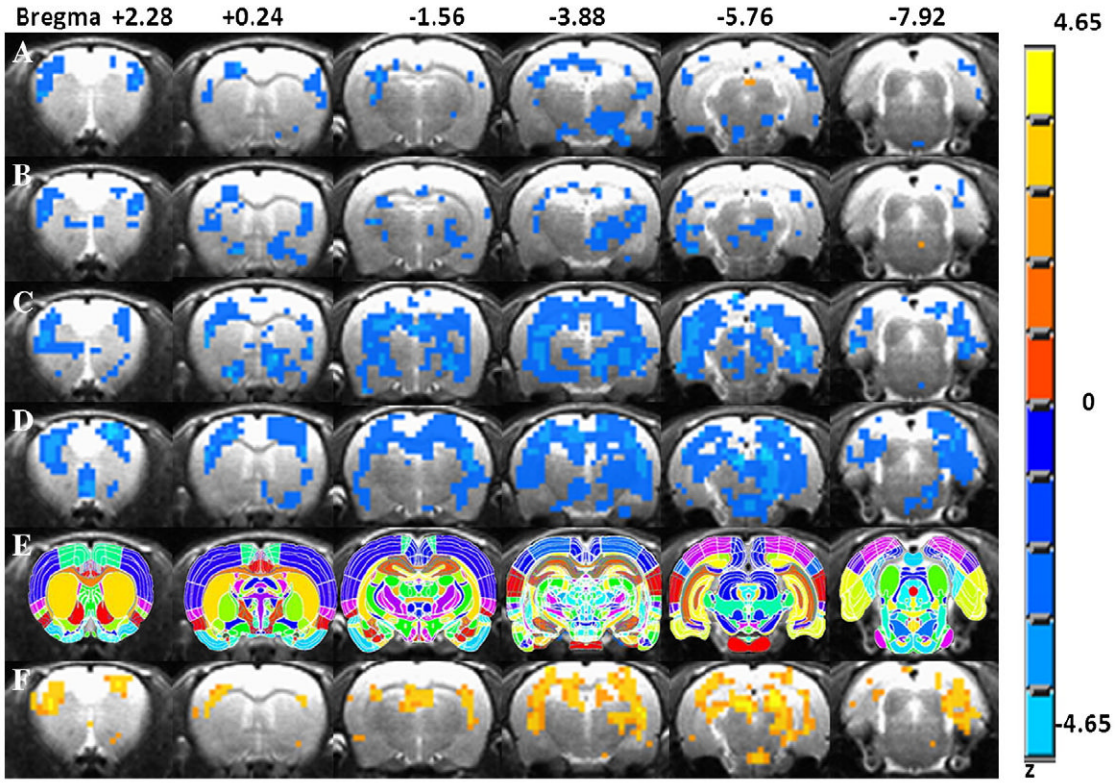

Fig. 3.

Dose-dependent activation maps of *l*-THP from initial *l*-THP injection compared with the 5-min pre *l*-THP injection. (A) Activation maps in AUC% with a dose of 5 mg/kg. (B) A dose of 10 mg/kg. (C) A dose of 20 mg/kg. (D) A dose of 40 mg/kg. (E) Anatomy of regional segmentation as the template for image localization processing with MIVA software. (F) Dose-dependent maps obtained with one-way ANOVA test. The color bar shows the *z* value of the maps (excluding row E). The right side of image is the left side in anatomy, the radiological convention.

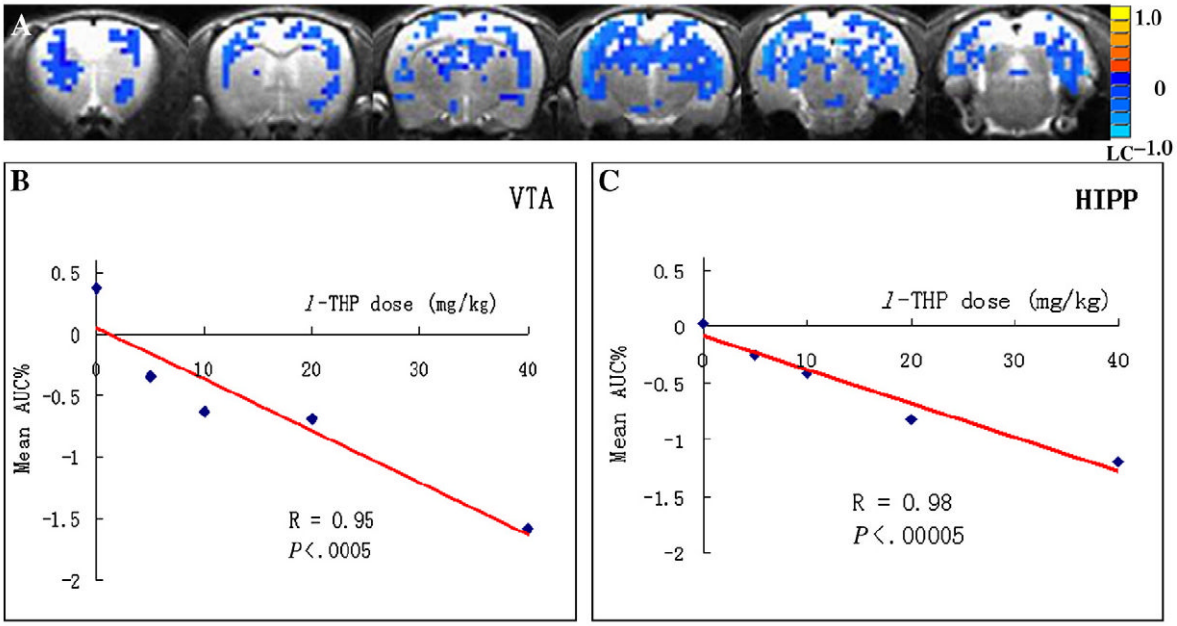

Fig. 4.

Linear correlation of *l*-THP doses and mean AUC% values. (A) The voxelwise linear regression maps of *l*-THP doses across the 16 rats. The regional mean AUC% values linearly correlated with *l*-THP doses in regions of VTA (B) and the HIPP (average for both left and right sides) (C).

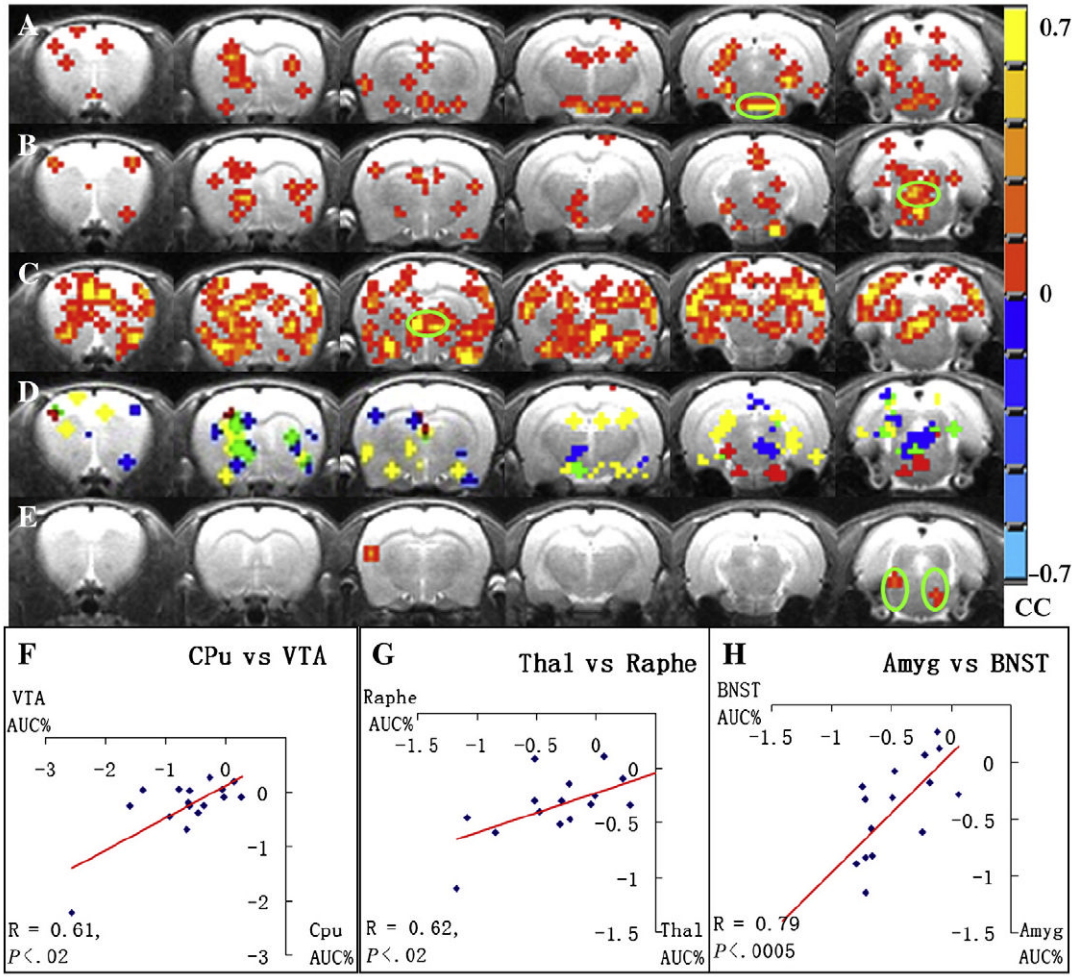

Fig. 5.

Pharmacological connectivity maps using four seed regions. (A) VTA connectivity maps. (B) Raphe nucleus maps. (C) BNST maps. (E). PPT maps. The cross-correlation coefficient (CC) values are displayed with the color bar shown on the right ($P<.05$); green circle indicates seed region location. (D) Common regions of A–C; red represents common areas of VTA and raphe connectivity maps; yellow represents the areas common to VTA and BNST maps; blue represents the areas common to raphe and BNST maps; green represents the areas common to all three maps. (F) Linear correlation between regional AUC% values in VTA and CPu in the dopaminergic connectivity. (G) The raphe nuclei and Thal in the serotonergic connectivity. (H) BNST and Amy related to noradrenergic connectivity.

Table 1

The pharmacological profile test results of *l*-THP

Receptor	Percent inhibition	Radioligand	K_d (M)
Adrenergic, a1A	55.78	[^{3}H]-7-meoxy-prazosin	4.0E–10
Adrenergic, a2A (h)	61.20	[^{3}H]-MK-912	0.5E–9
DA, D1 (hr)	97.34	[^{3}H]-SCH23390	2.0E–9
DA, D2 (hr)	87.37	[^{3}H]-spiperone	1E–10
DA, D3	82.92	[^{3}H]7-OH-DPAT	0.9E–9
Serotonin, 5HT1A (hr)	100.79	[^{3}H]8-OH-DPAT	0.8E–9
Serotonin, 5HT1D	75.89	[^{3}H]-5-CT	2.5E–9
Serotonin, 5HT4	73.60	[^{3}H]GR 113808	0.1E–9
Serotonin, 5HT7 (hr)	76.81	[^{3}H]-LSD	3E–9
Cannabinoid, CB1 (hr)	−5.64	[^{3}H]-CP 55940	0.6E–9
Muscarinic, M1 (hr)	4.65	[^{3}H]scopolamine,*N*-methyl	5E–11
Opiod, Mu (hr)	6.96	[^{3}H]-diprenorphine	2E–10

Receptors in bold letters indicate significantly high-binding affinity of *l*-THP. Percent inhibition of 50% or greater is taken as active binding. K_d values of radioligands are listed as reference in the far right column. H, human; hr, human recombinant. DPAT, Dipropylamino-tetrahydronaphthalen; CT, Carboxamidotryptamine; LSD, Lysergic acid diethylamide.

Table 2

Acute *l*-THP administration-induced regional average of AUC% at each dose level

ROIs	*l*-THP injection dosages (mg/kg)				
	0 (*n*=4)	5 (*n*=4)	10 (*n*=4)	20 (*n*=4)	40 (*n*=4)
NAc	0.01±0.04	−0.01±0.05	−0.16±0.02	−0.31±0.07	−0.35±0.09
SNR	0.17±0.04	−0.18±0.13	−0.26±0.16	−0.52±0.23	−1.01±0.22
Ins	−0.06±0.08	−0.29±0.05	−0.54±0.11	−0.62±0.24	−0.82±0.26
HIPP	0.02±0.02	−0.25±0.06	−0.42±0.22	−0.82±0.09	−1.20±0.24
IL	0.10±0.03	−0.03±0.03	−0.15±0.08	−0.35±0.07	−1.33±0.31
Motor cortex	−0.02±0.02	−0.20±0.05	−0.32±0.13	−0.52±0.04	−1.20±0.18
Somatosensory cortex	0.06±0.05	−0.15±0.07	−0.26±0.05	−0.48±0.55	−1.08±0.12
Auditory cortex	−0.00±0.13	−0.12±0.06	−0.31±15	−0.29±0.04	−1.28±0.23
Retrosplenium	−0.35±0.02	−0.31±0.12	−0.53±0.30	−1.28±0.42	−1.37±0.20
VTA	0.37±0.12	−0.34±0.08	−0.63±0.12	−0.69±0.18	−1.58±0.29
Hypoth	0.05±0.03	−0.29±0.11	−0.22±0.08	−0.63±0.09	−0.68±0.18
Thal	−0.04±0.02	−0.04±0.04	−0.38±0.05	−0.58±0.06	−0.94±0.15
Caudate putamen	−0.05±0.08	−0.32±0.15	−0.57±0.25	−0.91±0.07	−1.12±0.17
BNST	−0.08±0.05	−0.22±0.30	−0.48±0.28	−0.61±0.14	−0.75±0.32
Cl	0.01±0.03	−0.02±0.04	0.03±0.02	−0.04±0.03	−0.03±0.04

The first 14 regions (in BOLD letters), obtained from Fig. 3F, which demonstrated their dose-response activities (mean AUC%) to *l*-THP administration, as well as a nonresponsive region (Cl), are listed.